Atmospheric Thermal Lensing in Laser Resonators

Norman P. Barnes, Milfred E. Thomas, Grady J. Koch, and Waverly D. Marsh

Abstract—**Atmospheric absorption degrades laser performance both by absorbing laser energy within the laser resonator, which increases the loss, and by inducing a thermal lens in the atmosphere. Atmospheric thermal lensing can be quite severe, even when the absorption coefficient is quite modest. A model is developed which describes atmospheric thermal lensing; time constants, which are associated with the establishment and decay of the atmospheric thermal lens, are determined; experiments are performed using an injection seeded Ti:Al_2O_3 laser tuned to the H_2O absorption lines near 0.815 μm to validate the model; dependence of the atmospheric thermal lens on the laser energy and absorption coefficient were measured and found to agree with the model. In addition, the decay of the atmospheric thermal lens with time was measured and also found to agree with the model predictions.**

I. Introduction

ATMOSPHERIC thermal lensing can cause significant degradation of laser performance, even in cases where the absorption coefficient is relatively modest. It is generally known that atmospheric absorption can prevent laser oscillation at wavelengths corresponding to strong atmospheric absorption features [1], [2]. Often, this can be attributed to absorption of the laser radiation, providing an additional loss and therefore a predilection for laser operation at a different wavelength. However, the atmospheric absorption can also cause significant thermal lensing. Since atmospheric thermal lensing forms a negative lens, a resonator suffering from this effect can become unstable with a concomittant decrease in the performance of the laser.

Atmospheric thermal lensing is often undetected, since lasers most susceptible to these effects operate with narrow spectral bandwidths and with a short time interval between pulses. Atmospheric thermal lensing was observed in a laser used for a differential absorption lidar (or DIAL) experiments. In this case, the laser was spectrally narrowed and tuned exactly to an atmospheric absorption feature, albeit a relatively weak absorption feature [3]. As DIAL measurements usually attempt to sample the same volume of the atmosphere with both pulses, a moving platform for the DIAL instrument necessitates two pulses closely spaced in time, a 400 μsec separation for this particular case. However, atmospheric thermal lensing can be observed under a variety of experimental conditions other than the one described here, such as high pulse repetition frequency lasers.

Manuscript received September 13, 1994; revised December 15, 1994.

N. P. Barnes and G. J. Koch are with the NASA Langley Research Center, Hampton, VA 23681 USA.

M. E. Thomas is with the Science and Technology Corporation, Hampton, VA 23666 USA.

W. D. Marsh is with the Science Applications International Corporation, Hampton, VA 23666 USA.

IEEE Log Number 9409842.

Thermal lensing in solids has been observed and is a well understood phenomenon. Thermal lensing in solid state laser rods has been explored both theoretically and experimentally [4]–[6]. In this case, the laser rod is considered to be an uniformly heated cylinder which is cooled on its lateral surfaces. As such, the temperature profile is parabolic which leads to simple lensing. In fact, the deposition of heat in the laser rod may not be strictly uniform; however, the uniform heat deposition approximation is often utilized. Thermal lensing in nonlinear optical materials has also been observed [7]. In this case, the heat deposition often is no longer uniform. Since beams with Gaussian spatial profiles are often used, a Gaussian heat deposition profile can be used. Using such a heat deposition profile, the thermal lensing problem has been solved for lensing in nonlinear optical materials [8].

Atmospheric thermal lensing is considerably different than thermal lensing in solids, since atmospheric thermal lensing depends critically on the spectral content of the laser. Heat generation in solid state laser materials is usually associated with the optical pumping process. Since the thermal lensing depends on the absorption wavelengths rather than the lasing wavelength, the thermal lens is independent of the laser wavelength or linewidth. On the other hand, atmospheric thermal lensing depends critically on the specific laser wavelength and the spectral bandwidth. As a point in fact, atmospheric thermal lensing did not become obvious in the experiments performed here until the laser was narrowed through the introduction of a seed laser.

Thermal lensing in the atmosphere is also considerably different then thermal lensing in solids because of the time constants involved. For nominal laser rod radii of a few millimeters, the thermal diffusion time constant in a typical solid state laser material is on the order of a second. In this case, even lasers at low pulse repetition frequencies experience thermal lensing, and thermal lensing depends on average power. On the other hand, it will be shown that atmospheric thermal lensing time constants for the same beam radii are considerably shorter, on the order of several milliseconds. Consequently, atmospheric thermal lensing can disappear between pulses, even if the pulse repetition frequency is tens of Hz. Given this, atmospheric thermal lensing depends primarily on the energy of the previous pulse rather than on the average power.

In Section II of this paper, a model is developed to describe the atmospheric thermal lensing phenomenon. Included in the model is the atmospheric absorption, heat deposition in the atmosphere, and the subsequent thermally induced lensing. In addition, the time constants associated with the establishment and decay of the thermal lens are determined. In Section III,

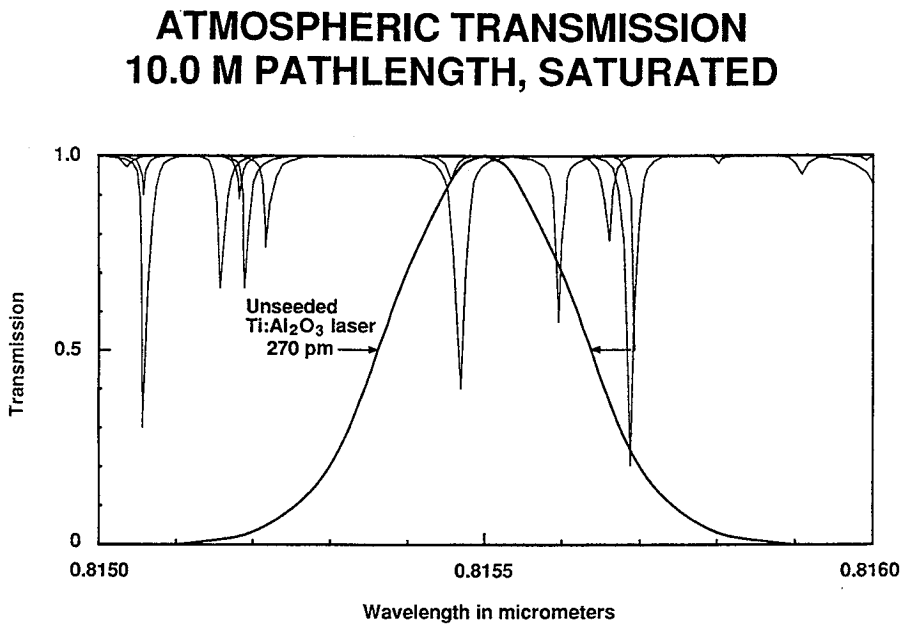

Fig. 1. Atmospheric transmission in the vicinity of 0.815μm with typical spectrum of an unseeded Ti:Al_2O_3 laser.

the experimental arrangement used to demonstrate atmospheric thermal lensing is described. Details on the Ti:Al_2O_3 laser used for these demonstrations as well as the method of measuring the atmospheric thermal lensing are provided. In Section IV, the results of the experiments are presented and reduced in order to compare them with the model. Experimental results are found to support the model in all of the aspects investigated. Finally, in Section V, the results are summarized.

II. Model

Atmospheric absorption features are relatively narrow which often confines the observation of atmospheric thermal lensing effects to line narrowed lasers. Of the normal atmospheric constituents, those which are most likely to contribute to atmospheric thermal lensing are H_2O and CO_2. Major constituents, N_2 and O_2, are homonuclear molecules which have small dipole moments and thus do not have strong absorption features in the visible to mid infrared region. Ar, as well as the much rarer He and Ne, appears only in the atomic form, which automatically excludes molecular absorption features in the visible to mid infrared region. H_2 has a low abundance and is a homonuclear molecule as well. As such, the H_2 absorption features are weak. On the other hand, CO_2 and H_2O occur in reasonable abundances and possess relatively strong dipole moments and concomitantly stronger absorption features. The linewidths are relatively narrow, however, on the order of 2.5 GHz for the H_2O lines considered in these experiments. Since longitudinal mode spacings are on the order of 0.2 GHz for typical resonators, only a few longitudinal modes near the center of the absorption feature will contribute strongly. Thus, atmospheric thermal lensing is most likely to be observed in line narrowed lasers.

Thermal lensing of broad-band lasers can also be described using the formalism developed here, but a suitably averaged absorption coefficient would have to be employed. A typical atmospheric transmission spectrum [9] appears in Fig. 1 along with the spectrum of an unseeded Ti:Al_2O_3 laser. As can be seen, only a fraction of the Ti:Al_2O_3 power would be absorbed even if the atmospheric absorption did not cause holes in the power spectrum.

TEM_{00} mode beams create Gaussian temperature profiles by the absorption process. Consider the case where a collimated TEM_{00} mode beam, characterized by a beam radius w_p at the exp (-2) intensity point, is propagating in a laser resonator. Given an atmospheric absorption coefficient, β_a, the heat deposited per unit volume as a function of the radial coordinate, $H(\rho)$, can be approximated by neglecting the variation of the photon density with longitudinal position as

$$H(\rho) = \frac{2E_{LI}\beta_a}{\pi w_p^2} \exp\left(\frac{-2\rho^2}{w_p^2}\right)$$

where E_{LI} is the laser energy internal to the resonator. Rather than using the internal laser energy, the laser output energy E_{LO} can be used, since it is an easily measurable quantity. Internal laser energy can be related to the laser output energy for reasonable mirror reflectivities [11] by

$$E_{LI} = \frac{1+R_m}{1-R_m} E_{LO}$$

where R_m is the reflectivity of the output mirror. Given this deposited energy density, the temperature will increase by an amount equal to

$$\Delta T = H/\rho_a c_p$$

where ρ_a is the density of the air and c_p is the specific heat.

A Gaussian temperature profile in turn creates a variation in the optical path length which is characterized by a similar profile. Denoting the variation in the optical path length by δ

$$\delta = (nl - n_0 l_0)$$
$$\approx \frac{\partial n}{\partial T} l \Delta T$$

where l is the physical path length and n is the refractive index, while l_0 and n_0 are the corresponding quantities of the unperturbed resonator. For air, the refractive index varies approximately as the density of the air [10]. Since the refractive index of air is so close to unity

$$n - 1 = AN$$

where A is a constant and N is the number density of air molecules. Using the ideal gas law

$$N = p/kT_a$$

where p is the pressure, k is Boltzmann's constant and T_a is the temperature. Substituting and differentiating

$$\frac{\partial n}{\partial T} = -\frac{Ap}{kT_a^2} = -\frac{n-1}{T_a}.$$

Combining the above equations, the variation of the optical path length caused by the absorption of laser energy becomes

$$\delta = \frac{-2\beta_a l E_{LI}}{\rho_a c_p \pi w_p^2} \exp\left(\frac{-2\rho^2}{w_p^2}\right) \frac{n-1}{T_a}.$$

An effective focal length will result from the variation of the optical path length with radial position. An effective focal length can be approximated by evaluating

$$\frac{\partial \delta}{\partial \rho} = -\frac{\rho}{f}$$

where f is the effective focal length. Evaluating the derivative and combining the above equations yields

$$\frac{1}{f} \approx \frac{-8\beta_a l E_{LO}}{\rho_a c_p \pi w_p^4} \frac{n-1}{T_a} \frac{1+R_m}{1-R_m}.$$

Since the refractive index of air decreases as the temperature increases [10], the atmospheric thermal lens is negative. Since the effective focal length is proportional to the beam radius to the fourth power, laser beams with small beam radii can be acutely affected. Simple lensing is described by the equation above. In fact, the atmospheric thermal lens will have some spherical aberration which will change the effective focal length somewhat. For experiments where the probe beam is smaller than the beam causing the heating, this approximation is valid since spherical aberration for a small beam is small. For larger beams, the spherical aberration will cause a change in the focal length by a factor of ln 2 [8].

While the optical path length will vary because of the energy deposited by the laser pulse, the atmospheric thermal lens will not occur immediately. Refractive index depends on the density of the air. However, the density requires time to respond to the deposited energy. Typically, the energy will be deposited in vibrational modes of the absorbing molecule. In general, the modes will probably be a combination of vibrational and rotational modes. Vibrational energy in these energetic modes will be converted into translational energy of the molecules which will then rearrange themselves to reflect the new temperature profile. Because of the high rate of molecular collisions, conversion of the vibrational energy to translational energy will occur relatively quickly. Therefore, in most cases, the time constant for establishing the variation in the optical path length is limited by the time interval required for the molecules to rearrange themselves. An estimate of this time interval is on the order of w_p/v_a, where v_a is the acoustic velocity in air, approximately 340 m/sec. For a beam radius of 1.0 mm, the time constant is about 3 μsec. Thus, for most Q-switched laser pulses, the pulse is gone before the atmospheric thermal lens is established. Normal mode pulses, however, could experience a transient atmospheric thermal lensing effect.

Decay of the atmospheric thermal lens is controlled by the diffusion of heat out of the volume occupied by the laser beam. Since the laser beam radius is small compared with the length of the laser resonator, thermal diffusion will occur radially outward from the initial volume in which the heat was deposited. In this case, the diffusion equation for the change in temperature ΔT can be written as

$$D\left(\frac{\partial^2 \Delta T}{\partial x^2} + \frac{\partial^2 \Delta T}{\partial y^2}\right) = \frac{\partial \Delta T}{\partial t}$$

where D is the thermal diffusion constant. A solution to this equation is

$$\Delta T = \frac{A}{(t_0 + t)} \exp\left(-\frac{x^2 + y^2}{4D(t_0 + t)}\right)$$

where A and t_0 are constants. Since the initial temperature distribution, after the absorbed energy is converted to heat, is

$$\Delta T = \frac{2\Delta T_0}{\pi w_0^2} \exp\left(-\frac{2(x^2 + y^2)}{w_0^2}\right)$$

the constants A and t_0 can be evaluated. Thus

$$\Delta T = \frac{\Delta T_0 w_0^2}{(w_0^2 + 8Dt)} \exp\left(-\frac{2(x^2 + y^2)}{(w_0^2 + 8Dt)}\right)$$

and thermal diffusion in this case can be well characterized by a time dependent beam radius given by

$$w_p^2 = w_{p0}^2 + 8Dt$$

where w_{p0} is the initial beam radius and D is the diffusion constant for air. For a beam radius of 1.0 mm, the decay time constant is about 6 msec. Thus, for pulse repetition frequencies on the order of 10 Hz, the atmospheric thermal lens has largely decayed before the next pulse occurs. For pulse pairs with a temporal separation of less than a millisecond, however, the second pulse will experience the atmospheric thermal lens created by the first pulse.

Atmospheric thermal lensing could significantly increase the beam divergence of the transmitted pulses. External to the laser resonator, the effective thermal length of a collimated beam propagating over a length l is

$$\frac{1}{f} \approx -\frac{8\beta_a l E_{LO}}{\rho c_p \pi w_p^4} \frac{n-1}{T_a}.$$

As the beam propagates, the diffraction will cause the beam to expand. If the absorption is weak, the expansion of the beam causes the majority of the atmospheric thermal lensing to be concentrated near the transmitting apertures. Thus, the

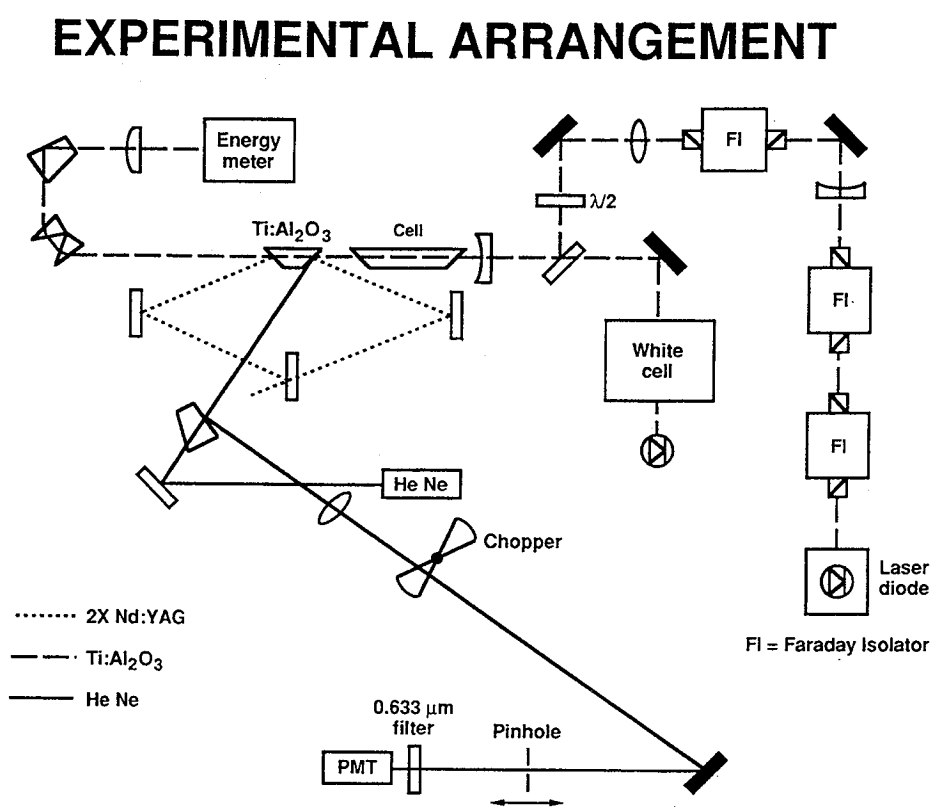

Fig. 2. Experimental arrangement of system for measuring atmospheric thermal lensing.

atmospheric thermal lens can be approximated by extending the limits of integration to infinity, that is

$$\frac{1}{f} \approx -\frac{8\beta_a E_{Lo}(n-1)}{\rho c_p \pi T_a} \int_0^\infty \frac{dz}{w_p^4}.$$

For Gaussian beam, the beam expands as

$$w_p^2 = w_{p0}^2(1 + (\lambda z/\pi w_{p0}^2)^2).$$

Substituting and integrating yields

$$\frac{1}{f} \approx -\frac{8\beta_a E_{LO}(n-1)}{\rho c_p \pi T_a} \left(\frac{\pi}{2w_{p0}}\right)^2 \frac{1}{\lambda}.$$

For small beams, beam radii on the order of 1.0 mm, even relatively weak absorption can create a significant negative lens. A negative lensing effect would increase the divergence of the transmitted pulse.

III. Experimental Arrangement

A $Ti:Al_2O_3$ resonator, similar to the lidar transmitter in which the effect was first observed, is used to experimentally investigate atmospheric thermal lensing and is diagrammed in Fig. 2. A glass cell with Brewster angle windows is placed in the laser resonator to introduce a controlled amount of water vapor in the laser resonator. The $Ti:Al_2O_3$ is line narrowed and stabilized by injection seeding with a laser diode [12], [13]. The injection seed source, and hence the $Ti:Al_2O_3$ laser, is precisely tuned and locked to a water vapor absorption line by passing a sample of the seed laser's beam through a White cell [14] filled with water and establishing a feedback loop to the laser diode current based on a frequency modulation locking technique [15]. A shift in the focus of a HeNe laser beam, made collinear with the $Ti:Al_2O_3$ laser mode volume, indicates the presence of an atmospheric thermal lens.

The $Ti:Al_2O_3$ laser is an unstable J shape resonator design consisting of symmetrically oriented dual $Ti:Al_2O_3$ bricks, although only a single brick is shown in Fig. 1 for the sake of clarity. It produces 40 mJ at 10 Hz with a pulse length of approximately 20 ns, and spectral bandwidth of approximately 270 pm at full-width-half-maximum. Beam quality of the laser is 1.5-2 times diffraction limited with >0.9 Gaussian correlation coefficient in both near and far fields. A graded reflectivity mirror, GRM, serves as the output coupler. Radii of curvature of the mirrors are 6 and -7 m for the highly reflecting HR and graded reflectivity mirrors. The GRM output coupler has a parabolic reflectivity profile with a center reflectivity of 0.50 and a tapered reflectivity at the mirror edge to minimize diffraction effects. The GRM output coupler forces the resonator to operate with a profile which closely approximates a Gaussian beam profile internal to the resonator. A highly reflecting HR mirror with 0.02 transmission at the seed source wavelength is used to allow a small throughput of the seed beam into the resonator.

Pumping the $Ti:Al_2O_3$ laser is accomplished with the second harmonic of a Q-switched Nd:YAG laser. This laser produces 300 mJ at 0.532 μm with a pulse repetition frequency of 10 Hz and 7-8 ns pulse length. Gaussian correlation coefficient in the far field is >0.95; the beam diameter is 6 mm with a full angle divergence of 0.45 mrads at exp(−2) of peak energy density. The pump beam is split into two equal beams and focused to a

2 mm spot using a 2-m focal length planoconvex lens, giving a fluence level at each Ti:Al_2O_3 brick of 9.1 J/cm^2.

Seeding the Ti:Al_2O_3 laser is done with a GaAlAs laser diode. Continuous wave single mode output of the diode is 100 mW at a center wavelength of 0.813 μm. Coarse wavelength tuning is accomplished with temperature; the temperature tuning characteristic is 60–70 pm/C°. Current tuning at a rate of 3.1 pm/mA allowed for fine tuning. Feedback sensitivity of the diode requires a minimum of 90 dB of isolation; three Faraday isolators are used in series to accomplish this isolation. It is necessary to orient beam splitter cubes of each stage to get maximum throughput and isolation. Finally a half wave plate polarizer is used to rotate polarization to the horizontal axis before entering the HR mirror of the Ti:Al_2O_3 laser. Proper injection seeding requires mode matching with a -0.5-m focal length biconcave lens and a 0.75-m focal length planoconvex lens placed 0.55 m and 0.95 m, respectively, from the diode housing. To accomplish seed alignment with the Ti:Al_2O_3 oscillator, a CCD TV camera and iris aperture is used. The iris aperture is placed in one leg of the resonator. The retro-reflected image of the IR beam is imaged on either side of the iris by the CCD TV camera. Care was taken to position the aperture axis in the resonator and maintain lasing using an XY translation stage.

A 5.0 mW HeNe is utilized as the source to detect thermal lensing because of its long coherence length and beam quality. The HeNe beam was made collinear with the mode volume of the Ti:Al_2O_3 oscillator by reflecting it off one of the Ti:Al_2O_3 bricks. Double passing the beam through the vapor cell increased the lensing effect. The return beam is reflected from a wedge and focused by a 1 m lens into the photomultiplier tube, PMT. Ambient light is prevented from entering the PMT with a 0.632 μm narrow band filter.

Beam radius of the HeNe laser is determined by measuring the transmission of the beam through a pinhole of known size. Ten positions of the pinhole are used to gain enough data points to generate the graph depicting the amount of lensing with and without operation of the Ti:Al_2O_3 laser. Alignment of the pinhole with the HeNe laser is accomplished by maximizing the transmission of the laser beam through the pinhole prior to firing the Ti:Al_2O_3 laser. The optical noise created by the ambient light required the use of a lock-in amplifier. Using a lock-in amplifier, accurate alignment of the pinhole at each position with respect to the HeNe optical axis is achieved.

The water vapor cell is designed with Brewster windows at each end with two top ports to insert the water. A strip heater is wrapped around the glass tube and secured with aluminum foil tape. To prevent condensation, care is taken in wrapping the strip heater to maintain the temperature on the entrance and exit windows of the cell. Cell temperature is measured using a digital thermometer with a needle probe. The probe is suspended into the center of one port with a cork plug, the other port is loosely plugged to maintain the atmosphere. The cell is positioned with a translation stage into one resonator leg simultaneously observing the Ti:Al_2O_3 output energy with a power meter.

A sample of the laser diode seed beam is passed through a White cell [14] to ensure that the wavelength corresponds to a water vapor absorption line. The White cell is filled with 15 torr of water vapor at room temperature, and its mirrors are adjusted to provide a 10 m path length. A HITRAN-PC simulation showed over 30 absorption lines from 0.81 to 0.82 μm ranging in White cell transmission from 0.05 to 0.50 [9]. Each of these lines is approximately 3 pm wide at full-width-half-maximum. A pulsed wavemeter is used to precisely monitor the wavelength and to determine which absorption line is selected. The frequency modulation locking technique involves modulating the laser diode current, and therefore, the laser diode frequency at 50 MHz. Synchronous demodulation of the photocurrent, generated by the photodiode at the output window of the White cell, provides an error signal that indicates distance from an absorption peak. This error signal is fed back to the laser diode to maintain a lock on an absorption peak.

IV. Experimental Results

Effective focal lengths can be determined by measuring the transmission through a pinhole as a function of position of the pinhole. As shown in Fig. 2, a HeNe laser beam samples much of the same volume occupied by the Ti:Al_2O_3 mode. As such, it experiences the same thermal lensing which the Ti:Al_2O_3 experiences. Consequently, the beam propagation properties of the HeNe will vary with the laser output energy of the Ti:Al_2O_3 laser. Of the focusing elements experienced by the HeNe laser, the 1.0-m focal length lens is the strongest. But variations in the atmospheric thermal lens will cause perturbations in the position of the beam waist induced by the 1.0-m focal length lens. As the atmospheric thermal lensing effect becomes more pronounced this negative lensing effect will cause the beam waist to occur farther from the 1.0-m focal length lens. Consequently, maximum transmission through the pinhole will occur at increasingly larger distances from the 1.0-m focal length lens as the laser output energy or atmospheric absorption increases.

Transmission through a pinhole of known radius at a given position determines the beam radius at that position. For a circular aperture with radius a and centered on the laser beam, the transmission of a Gaussian beam, T, is given by

$$T = (1 - \exp(-2a^2/w^2)).$$

Thus, by measuring the transmission the beam radius can be determined as

$$(w/a)^2 = -2/\ln(1 - T).$$

Measurements of the transmission T were taken as a function of time with the initial time occurring simultaneously with the occurrence of the Ti:Al_2O_3 laser pulse. Thus, plots of $-2/\ln(1 - T)$ versus distance should vary as the normalized beam radius squared $(w/a)^2$.

Measurements of the beam radius at several positions can be used to determine the position of the beam waist which, in turn, can be used to determine the effective focal length of the atmospheric thermal lens. With Gaussian beam propagation, the beam radius squared varies quadratically with position. Using several measurements of the transmission through the

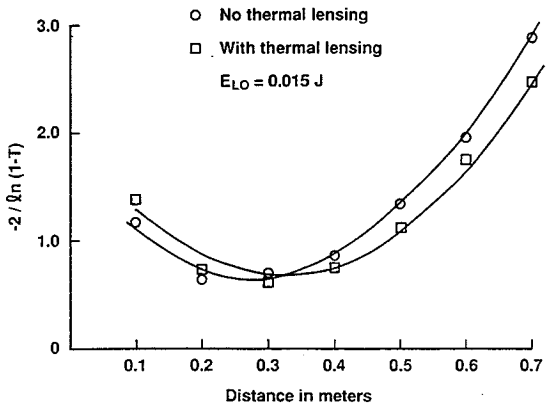

Fig. 3. Beam radius squared with and without atmospheric thermal lensing versus distance, laser output energy ≈0.015 J.

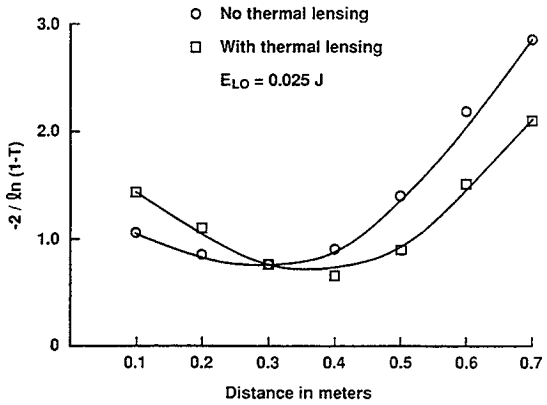

Fig. 4. Beam radius squared with and without atmospheric thermal lensing versus distance, laser output energy ≈0.025 J.

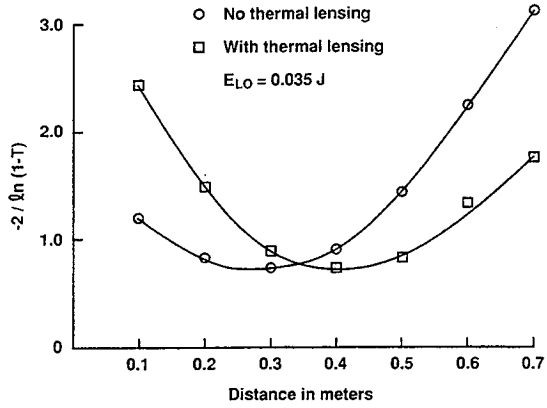

Fig. 5. Beam radius squared with and without atmospheric thermal lensing versus distance, laser output energy ≈0.035 J.

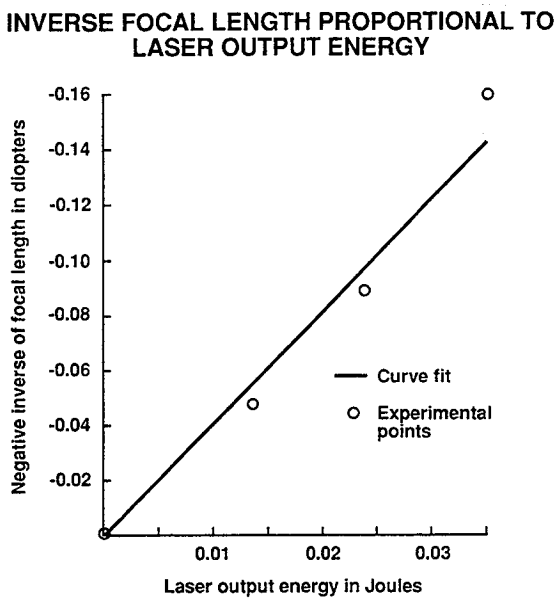

Fig. 6. Inverse of the effective focal length versus laser output energy.

aperture and a curve fitting procedure for a quadratic, the position of the beam waist can be determined. The position of the beam waist, with and without atmospheric thermal lensing, can then be used to determine the effective atmospheric thermal focal length by comparing the measured variation in the position of the beam waist with the results of Gaussian beam propagation calculations, with a variable negative lens representing the atmospheric thermal lens.

Experimental results are analyzed to verify the predicted dependence of the effective focal length on the laser output energy. A series of measurements of the transmission, through the pinhole as a function of pinhole position both with and without atmospheric thermal lensing, are taken at different laser output energies. Results are taken for a nominal laser output energy of 0.015, 0.025, and 0.035 J and are displayed in Figs. 3–5. As can be seen, the transmission through the pinhole does appear to vary quadratically with position of the pinhole. Differences in the position of the beam waist, with and without atmospheric thermal lensing, are then used to determine the effective atmospheric thermal focal length. The inverse of the effective atmospheric thermal focal length is then plotted versus the laser output energy in Fig. 6. As expected, the inverse of the effective atmospheric thermal focal length varies directly with the laser output energy. Given in the figure is the curve fit of the data to a direct relationship which yields a slope. A slope is also calculated using the model developed above. The ratio of the slopes is approximately unity, a factor of 1.04. Agreement between the model and the experimental results is highly encouraging, considering the data reduction necessary to extract the effective atmospheric thermal focal length.

Experimental evidence is in agreement with the model predictions that the inverse of the effective focal length is directly proportional to the absorption coefficient and length product. For equal laser output energies, the effective focal length is measured for two different concentrations of H_2O. For one concentration, the water vapor in room air is used in the cell and water vapor content is determined by measuring the relative humidity. For the other concentration, liquid water is injected into the cell and the cell is heated to 297°K. In this manner, the water vapor content could easily be changed by a factor of 2 or more. However, since the cell does not occupy the entire length of the resonator sampled by the HeNe laser, the absorption coefficient and length product had to be averaged over the length of the resonator sampled by the

TABLE I
COMPARISON OF MEASURED AND CALCULATED FOCAL LENGTH OF ATMOSPHERIC THERMAL LENS FOR TWO DIFFERENT H_2O CONCENTRATIONS

	INVERSE FOCAL LENGTH INCREASES AS ABSORPTION COEFFICIENT AND LENGTH PRODUCT			
Case	$\beta_a l$	E_{LO}	-1/f measured	-1/f calculated
1	$2.19 \cdot 10^{-3}$	0.035	0.159	0.142
2	$5.14 \cdot 10^{-3}$	0.035	0.333	0.334
Units		Joules	Diopters	Diopters

HeNe. Outside of the Ti:Al_2O_3 laser resonator, the atmosphere was not heated by the laser pulse and therefore does not affect the atmospheric thermal lensing. Results of the effective thermal focal length for the two different H_2O concentrations are listed in Table I. Again, the results of the model and the experiment come out to be in good agreement.

Transmission of the HeNe through the pinhole displays the characteristic time constants associated with the atmospheric thermal lensing. Transmission of the HeNe laser as a function of time are recorded by connecting the PMT directly to a digital oscilloscope. Oscilloscope traces are shown for six different positions of the aperture in Fig. 7. In Fig. 7, increasing transmission is in the downward direction, that is, away from the zero level which is also shown. In addition to the transmission through the aperture, the laser pulse can be seen as a single spike in the upper part of the individual oscilloscope traces. Immediately after the occurrence of the laser pulse, the transmission changes in a time which is short, compared with the 1.0 msec/div time scale of the oscilloscope. As the HeNe signal is weak due to the low reflectivity of some of the surfaces, the response time of the detection system was long, too long to accurately measure the rise time. A rapid change in the transmission is expected, based on the estimation of the time constant associated with the establishment of the effective thermal focal length. Afterwards, the transmission tends to return to its initial level with a time constant on the order of several milliseconds. Since the effective focal length is negative, the beam waist shifts away from the 1.0-m focal length lens. In keeping with this prediction, the transmission at shorter distances decreases initially while the transmission at greater distances increases initially.

Experiments support the model prediction that thermal diffusion is responsible for the atmospheric thermal lens. Rather than determining the position of the beam waist as a function of time, transmission through a fixed pinhole as a function of time can be investigated. In this way, inaccuracies associated with the determination of the position of the beam waist under the weak focusing occurring at later times are avoided. Transmission through the pinhole is then used to determine the beam radius at the position of the pinhole. As a comparison to the model, the beam radius at the pinhole is computed using Gaussian beam propagation calculations starting at the HeNe laser and including the effect of the atmospheric thermal lens.

Fig. 8 displays reasonable agreement between the measured and calculated beam radius squared as a function of time.

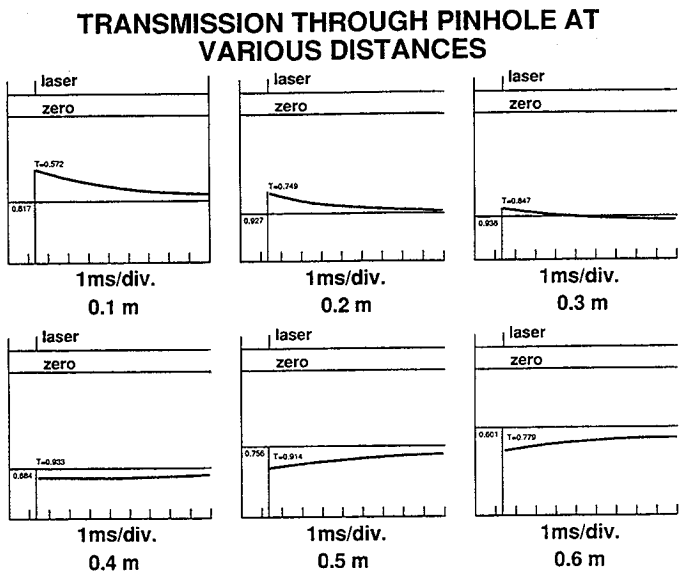

Fig. 7. Transmission through pinhole versus time for several different positions of the pinhole. The first position is closest to the 1.0-m focal length lens.

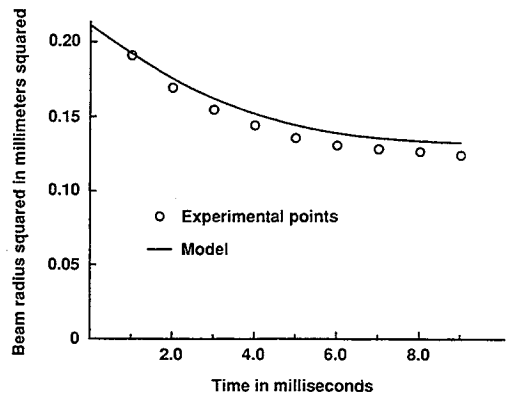

Fig. 8. Beam radius squared versus time. Open circles represent the experimental data while the line is the predictions of the model, normalized to produce initial agreement.

To concentrate on the temporal aspects of the problem, the initial atmospheric thermal lens is adjusted to reflect the actual initial transmission through the pinhole. For this experiment, an adjustment by a factor of 0.75 is required, somewhat larger than the accuracy inferred by the measurement of the atmospheric thermal lens as a function of laser output energy. However, a difference this large could result from a Ti:Al_2O_3 beam radius which is 0.93 as big as inferred from the measurements. As can be seen in Fig. 8, the model predicts the correct temporal variation of the beam radius squared; however, the decay is not quite as rapid as observed experimentally. Again, the difference could result from a beam radius, which is slightly smaller than the beam radius measurements indicate, by a factor of 0.88 in this case.

V. SUMMARY

A simple model has been developed to describe the effect of atmospheric thermal lensing. According to the model, the inverse of the effective focal length is directly proportional to

the laser output energy, as well as the absorption coefficient and length product, and inversely proportional to the beam radius to the fourth power. Even relatively weak absorption features can cause significant atmospheric thermal lensing if the laser is spectrally narrowed and tuned to the atmospheric absorption peak. In addition to intraresonator effects, atmospheric thermal lensing can cause a significant negative lensing of the transmitted pulse. This negative lensing can increase the divergence of transmitted pulses.

Time constants associated with the establishment and decay of the atmospheric thermal lens have been estimated. Establishment of the atmospheric thermal lens is probably limited by the time interval required for the atmosphere to adjust to the change in temperature, a time interval on the order of microseconds for nominal beam radii. Thus, a single Q-switched pulse will not be subject to the atmospheric thermal lens which it creates. Decay of the atmospheric thermal lens is controlled by the diffusion of heat radially outward from the initial beam profile, a time interval on the order of milliseconds for nominal beam radii. Consequently, the atmospheric thermal lensing effect will be most noticeable for closely spaced pulses.

Experiments were performed to verify the model using an injection seeded Ti:Al_2O_3 laser. Injection seeding was accomplished using a laser diode tuned to the H_2O absorption features near 0.815 μm. A White cell was used as a reference to keep the laser diode on the peak absorption of H_2O. Thermal lensing was measured by propagating a HeNe laser inside of the laser resonator and collinear with the Ti:Al_2O_3. Transmission through a pinhole of known size was used to determine the beam radius of the HeNe in the vicinity of the focus of a 1.0-m focal length lens. In turn, the measurement of the beam radius as a function of position, was used to determine the position of the beam waist. Position of the beam waist was used to determine the effective thermally induced focal length as a function of the laser output energy, as well as the absorption coefficient and length product. Transmission through a fixed pinhole as a function of time was used to determine the temporal decay of the effective focal length.

Experimental measurements of the effective focal length as a function of the laser output energy and absorption coefficient are in good agreement with the predictions of the model. Measurements of the shift in the position of the beam waist caused by a 1.0-m focal length lens are used to determine the atmospheric thermal lensing as a function of the laser output energy as well as the absorption coefficient and length product. In both cases, the agreement between the prediction of the model and the measurement is considered to be good, confirming that the inverse of the effective focal length dependence is directly proportional to the laser output energy as well as the absorption coefficient and length product.

Experimental measurements of the temporal behavior of the atmospheric thermal lens support the contention that thermal diffusion controls the decay. Measurements of the beam radius of the HeNe laser somewhat in front of the position of the beam waist as a function of time are compared with calculations of the beam radius as a function of time, using thermal diffusion to calculate the effective thermal focal length. Agreement between the measured and calculated beam radii is considered to be quite reasonable. A comparison indicates that the measured beam radius may be somewhat low.

REFERENCES

[1] J. Sienks, J. Eschner, V. M. Baev, and P. E. Toschek, "Sensitivity of intracavity absorption measurements with Ti:Al_2O_3 laser," *Opt. Commun.*, vol. 102, pp. 265–270, 1993.

[2] N. P. Barnes, K. E. Murray, M. G. Jani, and S. R. Harrell, "Diode pumped Ho:Tm:YLF laser pumping an $AgGaSe_2$ parametric oscillator," presented at the *Advanced Solid State Laser Conf.*, Salt Lake City, UT, 1994.

[3] J. C. Barnes, E. V. Browell, W. R. Vaughn, W. M. Hall, J. J. Degnan, R. D. Averill, J. G. Wells, D. E. Hinton, and J. H. Goad, "Development of a high altitude airborne DIAL system—the lidar atmospheric sensing experiment, LASE," in *Proc. 13th Int. Laser Radar Conf. NASA Conf. Pub.*, vol. 2431, pp. 6–9, 1986.

[4] W. Koechner, "Thermal lensing in a Nd:YAG laser rod," *Appl. Opt.*, vol. 9, pp. 2548–2553, 1970.

[5] L. Osterink and Foster, "Thermal effects in a Nd:YAG laser," *J. Appl. Phys.*, vol. 41, pp. 3656–3663, 1970.

[6] J. A. Williams-Byrd and N. P. Barnes, "Laser performance, thermal focusing and depolarization in Nd:Cr:GSGG and Nd:YAG," *SPIE, Solid State Lasers*, vol. 1223, pp. 237–246, 1990.

[7] C. J. Marquardt, D. G. Cooper, P. A. Budni, K. L. Schepler, and R. DeDomenico, "Thermal lensing in $AgGaSe_2$ OPO crystals," *Appl. Opt.*, vol. 33, pp. 3192–3197, 1994.

[8] N. P. Barnes and J. A. Williams-Byrd, "Average power effects in parametric oscillators and amplifiers," *J. Opt. Soc. Am.*, vol. 12, pp. 124–131, 1995.

[9] HITRAN, LOWTRAN, and FASCODE programs, which calculate the atmospheric transmission, can be ordered from the U.S. Dept. of Commerce, Na. Climatic Data Center of NOAA.

[10] M. Born and E. Wolf, *Principles of Optics*, New York: Pergamon Press, 1964.

[11] A. C. Selden, "Theoretical assessment of a high power continuous wave 4-level solid laser," *Brit. J. Appl. Phys.*, vol. 17, pp. 729–736, 1966.

[12] N. P. Barnes and J. C. Barnes, "Injection seeding I: theory," *J. Quantum Electron.*, vol. 29, pp. 2670–2683, 1993.

[13] J. C. Barnes, N. P. Barnes, L. G. Wang, and W. Edwards, "Injection seeding II: Ti:Al_2O_3 experiments," *J. Quantum Electron.*, vol. 29, pp. 2684–2692, 1993.

[14] J. U. White, "Long optical paths of large aperture," *J. Opt. Soc. Amer.*, vol. 32, p. 285, 1942.

[15] L. G. Wang, D. A. Tate, H. Riris, and Y. G. Gallagher, "High sensitivity frequency modulation spectroscopy with GaAlAs diode laser," *J. Opt. Soc. Amer.*, vol. B6, pp. 871–876, 1989

Norman P. Barnes, photograph and biography not available at the time of publication.

Milfred E. Thomas, photograph and biography not available at the time of publication.

Grady J. Koch, photograph and biography not available at the time of publication.

Waverly D. Marsh, photograph and biography not available at the time of publication.